Computational Tools for MRI-Guided Thermal Therapy

GEORGE ZOURIDAKIS and NITIN BAGRECHA
Department of Computer Science
University of Houston
501 PGH Hall, Houston, TX 77204-3010
USA

Abstract: - A graphical user interface (GUI) integrating several basic functions of an MRI-guided ablative thermal therapy procedure has been developed. The GUI features image processing and statistical analysis tools for treatment planning, target localization, continuous temperature monitoring, and verification of the procedure. An adaptive region detection algorithm is used for accurate target tracking, while thermal changes in the tissues are visualized by computing and superimposing temperature maps onto structural images. The GUI has significant potential for real-time control of thermal therapy, thus making it a safe and practical clinical tool for noninvasive treatment of soft-tissue tumors.

Key-Words: - MR Thermometry; Hyperthermia, Visualization; Imaging; Cancer; GUI.

1 Introduction

Local hyperthermia is a minimally invasive procedure offering a promising alternative to traditional surgery for the treatment of a variety of soft-tissue diseases. The objective is to coagulate a specified volume of tissue, usually a tumor, with minimal influence on the surrounding healthy tissues. Several modalities are used for thermal therapy, including high intensity focused ultrasound (FUS), interstitial lasers, as well as radio frequency and microwave applicators [6-18]. FUS is particularly attractive, since it is capable of noninvasively heating the focal area deep inside the body without significantly warming neighboring tissues. This reduces impact on patients, which in turn translates into reduced hospital stay and lower costs.

During the course of a procedure, magnetic resonance imaging (MRI) can be used to visualize temperature changes in the treated tissues by measuring the temperature-dependent proton resonance frequency (PRF) shift [1-3]. Moreover, the speed, accuracy, spatiotemporal resolution, and signal-to-noise ratio of the technique make thermotherapy procedures achievable in real-time.

The main objective of this project has been to develop a GUI that can aid in treatment planning, localization, monitoring, and verification during the ablative thermal therapy procedure. The various functions that the GUI can perform are summarized in Figure 1, and include modules for interaction with the MRI acquisition scanner, 3D image reconstruction and display at orthogonal and at arbitrary planes, image enhancement and analysis tools, such as plotting and equalization of histograms, image cropping, zooming, and color space transformation, selection of the region of treatment (ROT), calculation of temperature maps and total thermal dose delivered to the tissue in the ROT and the surroundings, color coding, and overlay on structural images, and finally the actions to be taken when healthy tissue surrounding the ROT is overheated.

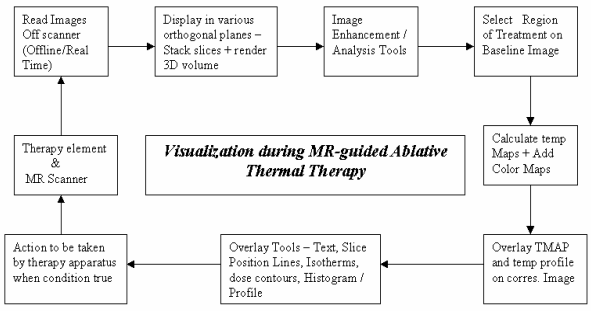

Fig. 1. Overview of the MR-guided ablative thermal therapy procedure controlled by the GUI.

2 Problem Formulation

Tissue heating is achieved by focusing energy in a specific region of the body using an external transducer. Sapareto and Dewey developed a method for thermal dose estimation for hyperthermia cancer therapy in 1984, based on a model of cell death with temperature by Arrhenius [4]. This method was subsequently modified for use in thermal ablation therapy for temperatures above hyperthermia temperatures (T = 43 °C). Dose can be

expressed in terms of equivalent time spent at a temperature of 43 °C using a discrete summation to approximate the cumulative effect of temperature history given by

$$t_{43}(n) = \sum_{t=0}^{n-\Delta t} R^{(43-T_n)} \Delta t \quad with R = \begin{cases} 0.25 & for \quad T_n < 43°C \\ 0.50 & for \quad T_n \geq 43°C \end{cases}$$

where R is an empirical constant and T_n the average temperature during time Δt.

Three temperature-dependent magnetic resonance parameters are most prominent for temperature monitoring and calculation of temperature maps, namely,

- The spin-lattice relaxation time, T1, which has a linear temperature dependency only over a limited range with significant deviations from linearity reported at high temperatures (> 50°C).
- The self-diffusion coefficient of water, D, which has a high theoretical temperature sensitivity of 2.4%/°C. But, because of the small scale of measurement and the strict SNR requirements, in vivo implementation of the diffusion-based method has been plagued by a tradeoff between artifacts and temporal resolution.
- The proton resonance frequency (RPF) shift of water has a temperature sensitivity (-0.01 ppm/°C) that varies linearly over a range of approximately 0 °C - 100°C making it useful for monitoring large temperature changes [1-3]. The temperature sensitivity is relatively tissue independent compared to other methods.

The established method of measuring these shifts rapidly with MR is phase-difference imaging, which measures the PRF shift indirectly rather than directly, using a series of complex phase-difference images acquired by a fast spoiled gradient-echo sequence on a GE 1.5T scanner. The temperature-dependent phase shift (Δϕ), which accumulates during echo time (TE), is proportional to the PRF shift (Δf). The latter is given by [1]

$$\Delta\phi = \Delta f \, TE = 2\pi \, \gamma Bo \, TE \, \alpha \, \Delta T,$$

where γBo is the resonance frequency (equal to 63.87 MHz at 1.5 T) and α is the temperature sensitivity coefficient of the material. Phase images acquired immediately before and during temperature elevation are subtracted to obtain the temperature change (ΔT). More specifically, the phase difference between two images is computed from [5]

$$\Delta\phi = \tan^{-1}\left(\frac{\mathrm{Re}_i \, \mathrm{Im}_{i-1} - \mathrm{Re}_{i-1} \, \mathrm{Im}_i}{\mathrm{Re}_{i-1} \, \mathrm{Re}_i + \mathrm{Im}_{i-1} \, \mathrm{Im}_i} \right),$$

where Re and Im are the real and imaginary parts, respectively, of the complex images acquires at time (*i*-1) and (*i*). This method eliminates the problem of phase wrapping.

The ongoing processing algorithm is summarized in Figure 2 and consists of the following steps, which are applied separately to each pixel of an image:

1. Compute a magnitude threshold based on a reference image.
2. Calculate the incremental complex phase difference (δϕ).
3. Compute a threshold for δϕ.
4. Sum δϕ to obtain a cumulative phase change (Δϕ).
5. Scale to temperature.
6. Calculate contribution to thermal dose [4].
7. Update thermal dose.

Magnitude and phase filters are employed to check whether each pixel in the tissue region corresponding to that pixel has been overheated. These filters optimize computation of the temperature maps in terms of accuracy and speed.

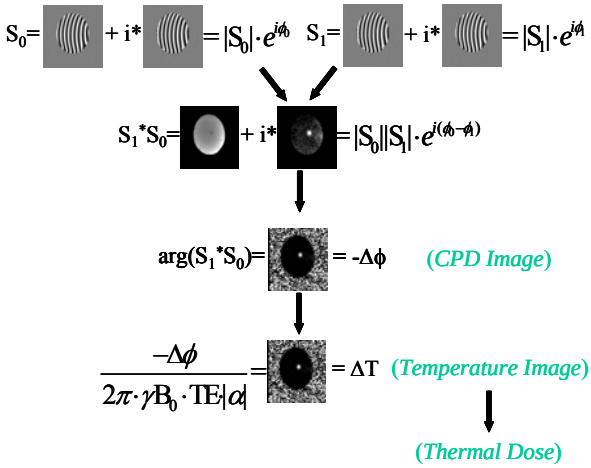

Fig. 2. Summary of the procedure used for computing the thermal dose.

Segmentation and tracking of the region of treatment (ROT) is carried out using a condensation algorithm based on a mixture-of-normals model at the pixel level. This is an adaptive method which separates

the image into foreground (ROT) and background (surrounding tissue) contributions [5].

3 Results

Figure 3 shows an example of the various functions that the GUI developed can perform, including image preprocessing, target selection, and treatment planning. Target coverage (the matrix of stars) is intentionally exaggerated for illustration purposes.

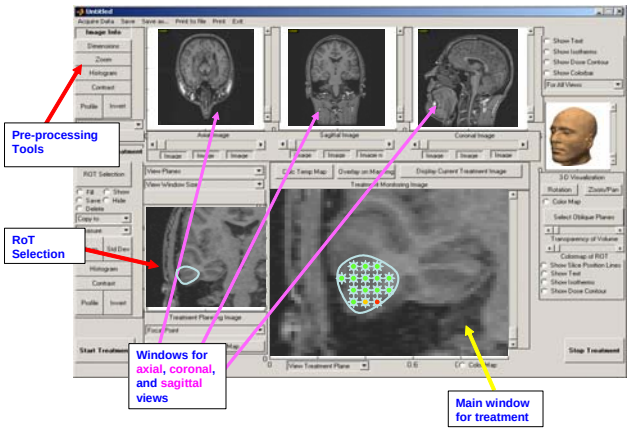

Fig. 3. Separate GUI areas for preprocessing, 3D image reconstruction, target selection, and treatment.

Figure 4 shows an example of a temperature map co-registered on the structural image of canine brain, and various windows available at the GUI. The temperature scale represents real temperatures reconstructed from MRI sequences.

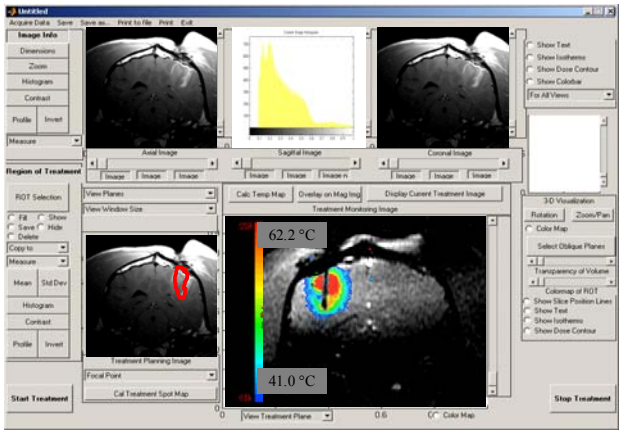

Fig. 4. Example of temperature map co-registered on a structural image of canine brain.

Figure 5 shows an example of treatment of canine brain tumors. Five canine brains were treated using a two-element, cooled ultrasound applicator. The total treatment times were 12 to 15 minutes at power levels of 4-12 W. The green isodose line correspond to an equivalent temperature t_{43} = 50 min. Verification with results from pathology shows good treatment coverage of the tumor area.

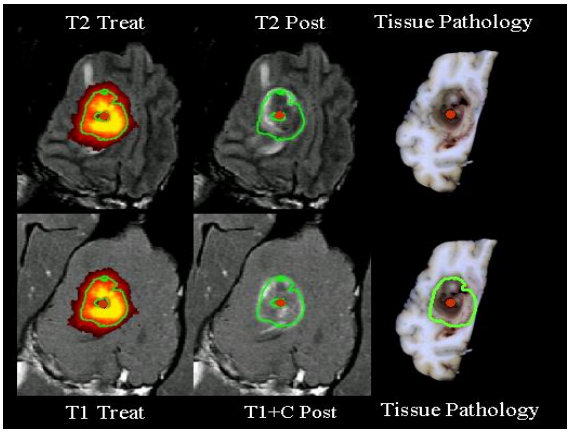

Fig. 5. Example of treating canine brain tumors. The isodose is t_{43}=50 min.

Figure 6 shows an example of guidance in canine prostate treatment, where maximum temperature, threshold temperature, and total dose are displayed, along with an enhanced structural image of the treatment area. The corresponding isodose at t_{43} = 90 min is shown in Figure 7.

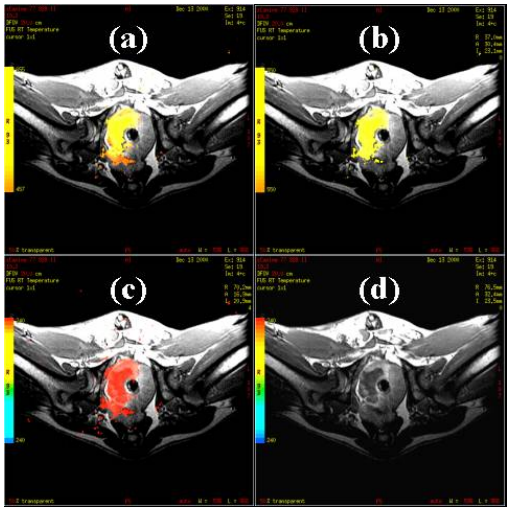

Fig. 6. Example of guidance in canine prostate; (a) maximum temperature - 45 ≤ T ≤ 65; (b) threshold temperature - T ≥ 55°C; (c) integral dose (Arrhenius) - t43 ≥ 240 min; (d) contrast-enhanced T1 MRI.

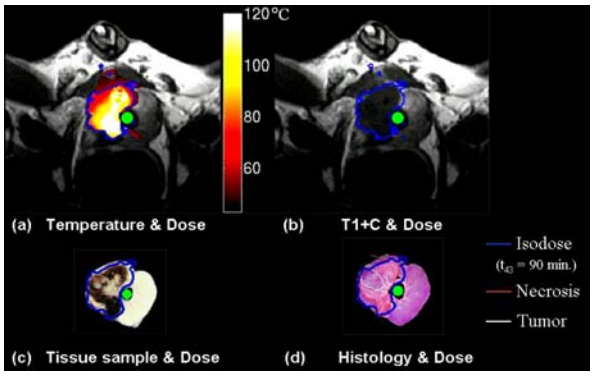

Fig. 7. Isodose in canine prostate

3 Conclusions

Preliminary results from this ongoing project are really promising, and demonstrate the feasibility of the proposed approach. However, several issues need further investigation, such as, for example, the algorithms for the construction of the temperature maps. The latter are typically very coarse and require some sort of filtering to obtain a smooth temperature image to be co-registered with the structural image. An example of the unprocessed maps is shown in Figure 8 below.

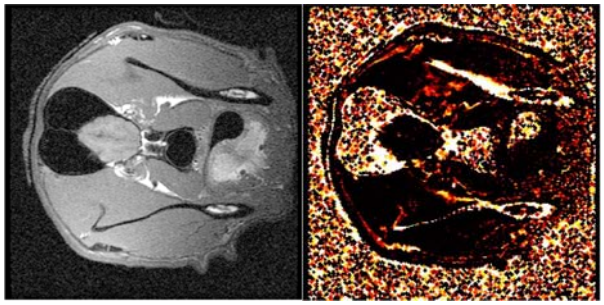

Fig. 8. Example of unprocessed temperature map (right) and the corresponding structural image (left).

The present implementation of image smoothing includes diffusion filtering and wavelet transform-based approaches to remove the noise, as well as masking to isolate the area of treatment.

Furthermore, to compute the thermal doses correctly, given the cumulative effect of tissue heating, we need to track in space and time (the temperature of) the various pixels, as shown in Figure 9, which is a very time consuming and CPU intensive procedure.

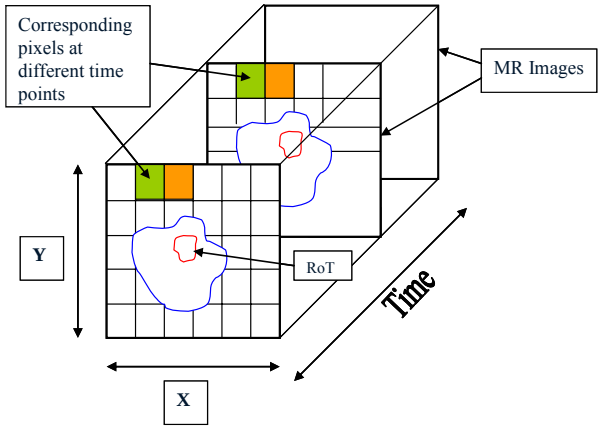

Fig. 9. Spatio-temporal tracking of pixels for filtering and temperature map computation purposes

Finally, with only a few exceptions, most of the results obtained thus far have been achieved with phantom and synthetic data, which were used to fine-tune the parameters of the various algorithms developed for the GUI. Finally, to achieve the long term objective of this line of research of an integrated tool for ablative thermal therapy, the GUI should be interfaced with the treatment apparatus to control the position and intensity of the focal point.

Thus, current efforts focus on the development and testing of alternative methods for the construction and smoothing of temperature maps, on validating our techniques with clinical data, and on optimizing the overall procedure so that execution time is decreased until eventually reaches real time.

5 Acknowledgement

Special thanks to Drs. R. J. Stafford and J. D. Hazle, Department of Imaging Physics, M.D. Anderson Cancer Center, The University of Texas, for providing the MRI data.

This work has been supported in part by a generous grant from the Texas Learning and Computation Center (TLC^2).

References:

1. Ishihara Y, Calderon A, Watanabe H, Okamoto K, Suzuki Y, Kuroda K, Suzuki Y. A precise and fast temperature mapping using water proton chemical shift. Magn Reson Med 1995;34:814-823.

2. Peter RD, Hinks RS, Henkelman RM. Ex vivo tissue-type invariability in proton-resonance frequency shift MR thermometry. In: Proceedings of the 5th Annual Meeting of ISMRM, Vancouver, Canada, 1997. P 1955.

3. Graham SJ, Bronskil MJ, Henkelman RM. Time and temperature dependence of MR parameters during thermal coagulation of ex vivo rabbit muscle. Magn Res Med 1998; 39:198-203.

4. Sapareto SA, Dewey WC. Thermal dose determination in cancer therapy. Int J Radiation Oncology Biol Phy 1984; 10:787-800.

5. Bagrecha N., Stafford R.J., Hazle J.D., Zouridakis G. MRI-based Temperature Tracking During Ablative Therapy: Development of a Graphical User Interface, 8th Annual Structural Biology Symposium, May 2003.

6. Olsrud J, Wirestam R, Brockstedt S, Nilsson AM, Tranberg KG, Stahlberg F, Persson BR. MRI thermometry in phantoms by use of the proton resonance frequency shift method: application to interstitial laser thermotherapy. Phys Med Biol. 1998; 43(9): 2597-2613.

7. Menovsky T, Beek JF, van Gemert MJ, Roux FX, Bown SG. Interstitial laser thermotherapy in neurosurgery: a review. Acta Neurochir (Wien). 1996; 138(9):1019-26.

8. Kahn T, Harth T, Kiwit JC, Schwarzmaier HJ, Wald C, Modder U. In vivo MRI thermometry using a phase-sensitive sequence: preliminary experience during MRI-guided laser-induced interstitial thermotherapy of brain tumors. J Magn Reson Imaging. 1998; 8(1): 160-164.

9. Rieke V, Vigen KK, Sommer G, Daniel BL, Pauly JM, Butts K. Referenceless PRF shift thermometry. Magn Reson Med. 2004; 51(6):1223-31.

10. Gewiese B, Beuthan J, Fobbe F, Stiller D, Muller G, Bose-Landgraf J, Wolf KJ, Deimling M. Magnetic resonance imaging-controlled laser-induced interstitial thermotherapy. Invest Radiol. 1994; 29(3): 345-351.

11. Bremer C, Allkemper T, Menzel J, Sulkowski U, Rummeny E, Reimer P. Preliminary clinical experience with laser-induced interstitial thermotherapy in patients with hepatocellular carcinoma. J Magn Reson Imaging. 1998; 8(1): 235-239.

12. Chen L, Wansapura JP, Heit G, Butts K. Study of laser ablation in the in vivo rabbit brain with MR thermometry. J Magn Reson Imaging. 2002; 16(2): 147-152.

13. Fiedler VU, Schwarzmaier HJ, Eickmeyer F, Muller FP, Schoepp C, Verreet PR. Laser-induced interstitial thermotherapy of liver metastases in an interventional 0.5 Tesla MRI system: technique and first clinical experiences. J Magn Reson Imaging. 2001; 13(5): 729-737.

14. Smith NB, Buchanan MT, Hynynen K. Transrectal ultrasound applicator for prostate heating monitored using MRI thermometry. Int J Radiat Oncol Biol Phys. 1999; 43(1): 217-225.

15. Weidensteiner C, Quesson B, Caire-Gana B, Kerioui N, Rullier A, Trillaud H, Moonen CT. Real-time MR temperature mapping of rabbit liver in vivo during thermal ablation. Magn Reson Med. 2003; 50(2): 322-330.

16. Carter DL, MacFall JR, Clegg ST, Wan X, Prescott DM, Charles HC, Samulski TV. Magnetic resonance thermometry during hyperthermia for human high-grade sarcoma. Int J Radiat Oncol Biol Phys. 1998; 40(4): 815-22.

17. Peller M, Kurze V, Loeffler R, Pahernik S, Dellian M, Goetz AE, Issels R, Reiser M. Hyperthermia induces T1 relaxation and blood flow changes in tumors. A MRI thermometry study in vivo. Magn Reson Imaging. 2003 Jun; 21(5): 545-551.

18. Wlodarczyk W, Boroschewski R, Hentschel M, Wust P, Monich G, Felix R. Three-dimensional monitoring of small temperature changes for therapeutic hyperthermia using MR. J Magn Reson Imaging. 1998; 8(1): 165-174.